Thin Solid Films 664 (2018) 83–89

Contents lists available at ScienceDirect

Thin Solid Films

journal homepage: www.elsevier.com/locate/tsf

Deposition of AlN films for acoustic biosensors by deep oscillation magnetron sputtering: effect of bias voltage

L. Melo-Máximo[a], J. Lin[b], A.E. Murillo[a], O. Salas[a,*], J. Oliva-Ramírez[a], J. Oseguera[a], B. García-Farrera[a], D. Melo-Máximo[a]

[a] Tecnológico de Monterrey-CEM, Carretera al Lago de Guadalupe km 3.5, Atizapán de Zaragoza, México 52926, México
[b] Southwestern Research Institute, 6220 Culebra Rd., P.O. Drawer, 28510 San Antonio, TX, USA

ARTICLE INFO

Keywords:
AlN
Deep oscillation magnetron sputtering
Acoustic biosensors
Piezoelectric thin films

ABSTRACT

The present study showed that Deep Oscillation Magnetron Sputtering (DOMS) has an excellent potential to produce AlN films for biosensing applications. However, careful control of the process parameters is required to attain the desired features. Al/AlN/Al films deposited via DOMS on Si wafers were extensively characterized to assess this potential. The resulting microstructures were examined by glancing angle x-ray diffraction, scanning electron microscopy coupled with energy dispersive microanalysis, atomic force microscopy, and x-ray photoelectron spectroscopy. The results indicated that there is a strong effect of the bias voltage (V_b) applied to the substrate on the structure of the Al/AlN/Al films and that it can be divided in two regimes. The low V_b regime produced the best features of the AlN films for the present application. These included a strong (002) orientation, low residual stress, and uniform surface roughness. In the high V_b regime, these features degraded. The effects were associated to the nature and energy of the impinging species as a function of V_b.

1. Introduction

Aluminum nitride in its hexagonal phase (h-AlN: wurtzite) exhibits a unique combination of properties including high values of hardness and stiffness, good thermal stability, good corrosion resistance, wide band gap, high sound speed, and piezoelectricity among others. As a result, a wide range of applications exists for this material from tribological to optical, electrical and electronic. In particular, for its use in acoustic biosensors, this material outstands due to its piezoelectric properties, which are optimized when its hexagonal structure is oriented along [001] (c-axis orientation).

In addition to having the proper orientation, it is desirable to minimize the thickness of the h-AlN to increase the sensibility of the acoustic sensors, in particularly for the FBAR type (Film Bulk Acoustic Resonators) [1,2]. Other requirements include good density and controlled residual stress to produce the required piezoelectric and dielectric properties [3]. For the biological response, it is anticipated that surface roughness and composition will play a role in the attachment of biomarkers on the surface of the sensor, particularly in the case of surface wave acoustic sensors [4,5]. Considering these requirements, a logical choice is to produce the piezoelectric AlN as deposited thin films, which indeed has already been done [1,6]. Within the deposition methods utilized, magnetron sputtering (MS) seems to offer the potential to achieve most of the requirements mentioned above. Additionally, MS is known for its compatibility with the microfabrication processes used for the production of the sensors [1].

There is a substantial number of studies aimed at producing piezoelectric AlN thin films by magnetron sputtering through all its variants. To mention a few examples in each category, the studies of Moreira et al. and Ababneh et al. [7,8] can be mentioned for direct current MS (d.c. MS), those of Singh et al. and Li et al. [9,10] for radiofrequency MS (r.f. MS), and the ones by Fu et al. and Lundin et al. [6,11] for high power impulse MS (HIPIMS). Good piezoelectric AlN thin films have been obtained by most of the MS techniques, but HIPIMS outstands due to its ability to produce readily films with high density, preferential orientation, and low roughness [11]. In HIPIMS, short pulses of high power are applied to the target in order to achieve high ion fractions in the plasma generated without excessive heating of the target. The high ion density can then be manipulated, mainly with a bias voltage applied to the substrate, to control the energy and mobility of the species during film formation and thus the structure and properties of the deposited film. A recent modification of the HIPIMS technique, DOMS, additionally offers the possibility of virtually arc-free deposition of various thin films [12]. In DOMS, the high power pulses

* Corresponding author.
E-mail address: osalas@itesm.mx (O. Salas).

https://doi.org/10.1016/j.tsf.2018.08.022
Received 5 March 2018; Received in revised form 25 July 2018; Accepted 7 August 2018
Available online 17 August 2018

are longer and contain a set of shorter, deep voltage oscillation pulses, which also produce high ionization fractions. The level and energy of the ions can be manipulated through the target peak current and voltage, respectively [13]. Additionally, the energy of the ion flux can also be controlled via a bias voltage applied on the substrate [14]. Furthermore, in contrast with conventional d.c. sputtering plasmas, in DOMS there is a high fraction of metallic ions reaching the substrate in addition to Ar ions. Due to their abundance, these ions not only favor the formation of denser films thus, but their interaction with the atoms in the growing film is more effective as they are of practically of the same size [14].

Lin J. et al. [15] have already successfully applied DOMS for the deposition of AlN thin films. They varied the peak current and thickness of the films and studied their effect of the properties of the films. In all cases a (002) AlN orientation was obtained without external heating or the use of a bond layer. Two deposition regimes were observed for both variables. In the lower peak current range, as this parameter increased, the (002) texture, and density of the films increased. However, past a critical current value, excessive ion bombardment resulted in poorer (002) orientation, higher compressive residual stresses and more film defects. In terms of thickness, at the lower values, films with very fine columnar structure, low c-axis orientation and high compressive stress were observed. Larger thickness led to the formation of films with stronger (002) texture and less compressive stress.

In the present study, the effect of a bias voltage applied on the substrate during deposition of Al/AlN/Al thin films on Si substrates by DOMS was investigated. As mentioned above, bias voltage can be used to control the characteristics of the ionized flux obtained in DOMS and thus tailor the structure of the films. The proposed film architecture simulates an eventual film structure to be used in a typical FBAR biosensor. The films were characterized with an emphasis on their orientation, structure, and surface roughness and morphology in order to explore the potential of DOMS deposition techniques to be involved in the eventual production of FBAR acoustic biosensors based on AlN piezoelectric thin films.

2. Experimental procedure

2.1. Deposition by DOMS

Seven films composed of a bottom Al layer, an AlN layer, and a top Al layer (b-Al/AlN/t-Al) were deposited via DOMS on Si (100) substrates. The depositions were carried out in a closed field unbalanced magnetron sputtering system (CFUBMS). The system has two rectangular unbalanced magnetrons (102 mm × 292 mm) facing one to another with a distance of 240 mm. Only one magnetron installed with a high purity (99.9%) Al target was used for the depositions. The Si (100) wafers were mounted on a substrate holder and installed 50 mm away from the target.

The chamber was heated at 250 °C and pumped down to a base pressure below 2×10^{-4} Pa prior to the deposition runs. The Si substrates were first cleaned using an argon (Ar) glow discharge plasma generated by biasing the substrates at a working pressure of 1.07 Pa using a pulsed voltage of −600 V (100 kHz and 80% duty cycle) for 30 min. After substrate cleaning, a ~200 nm Al bond layer was deposited by sputtering the Al target in pure Ar. After that, N_2 was fed into the deposition system to form the AlN films. The Al target was powered by deep oscillation magnetron sputtering (DOMS) (Zond, Inc.) at a constant average power of 1.0 kW (power density of ~5.3 W/cm^2). The peak voltage, peak current and pulsing frequency were adjusted in each run to keep the average power constant. The frequency of the oscillation pulse was kept constant. The Ar and N_2 flow rates were maintained at 50 sccm and 21 sccm, respectively, to maintain a constant working pressure of 0.67 Pa. Different substrate bias voltages (V_b), including ground, floating, and − 30 V to −150 V were applied for the depositions. The parameter details for each run are presented in Table 1. Fig. 1 shows the typical waveforms for the long pulses and the deep oscillations. After the AlN layer deposition, a ~200 nm Al layer was deposited as an outer layer for the entire coating in the same conditions as the AlN layer. The total deposition time was 120 min. Both, the bond and top Al layers, were deposited with the same bias voltage as the AlN films.

2.2. Film characterization

Characterization of the samples was similar to that carried out in a previous study [16] and included scanning electron microscopy (SEM) coupled with energy dispersive microanalysis (EDS), glancing angle X-ray diffraction (GAXRD), atomic force microscopy (AFM) and X-ray photoelectron spectroscopy (XPS). SEM and EDS were performed in a JEOL 6360LV equipment. In order to obtain cross-sectional views of the films, some scratches were carefully produced with a fine, sharp knife in some locations in the films. GAXRD was carried out at 40 kV and 25 mA with Cu-Kα radiation in a Bruker D8 ECO-ADVANCE diffractometer. Two times steps were used: 0.5 s and 1 s and an x-ray incidence angle of 0.5°. Atomic Force Microscopy (AFM) was performed in air with a Bruker BioScope Catalyst apparatus (Santa Barbara California, USA), using ScanAsyst mode, and RTESP model probes (Camarillo California, USA), scan rate 1 Hz.

For XPS, an ultra-high vacuum (UHV) Scanning XPS microprobe PHI 5000 VersaProbe II from Physical Electronics was used. An Al K X-ray source ($h\nu$ = 1486.6 eV) was applied at 25 W and with an MCD analyzer. At 45° to the normal surface the spectra were captured in a constant pass energy mode (CAE) for survey surface of E_0 = 117.40 eV and high-resolution narrow scan of 11.75 eV. A reference to the background silver $3d_{5/2}$ photopeak at 368.20 eV was done for the peak positions obtaining a FWHM of 0.56 eV, C 1 s hydrocarbon groups and Au $4f_{7/2}$ at 285.00 eV and 84.0 eV respectively.

3. Results and discussion

Fig. 2 presents the secondary electron images from the surface and cross section of the seven samples. In the cross sectional views, mainly the AlN from the b-Al/AlN/t-Al films can be observed, while in the surface views evidently only the t-Al film could be analyzed. In these views, a non-monotonic variation of the t-Al surface roughness with substrate bias was observed. Starting with the sample produced at ground potential (Si1), the surface roughness first decreased, reaching a minimum for V_b = -60 V (Si4) and from this point it increased rapidly with higher negative substrate voltage. The higher magnification views on the right show that the surface of all the samples was composed of granules protruding on flatter regions. In the smoother films, produced at the lower V_b values (Si1-Si4), the granules were very small and uniformly distributed over the surface. These samples did not show cracking or detaching of the films indicating a low level of residual stress and good adhesion. The pits observed on the Si surface in sample Si1 have been observed before and corresponded to Si diffusion into the Al bottom layer [17]. In the films deposited at the higher - V_b values, Si5 to Si7, agglomerations of large nodules developed, which were the origin of the higher surface roughness. For the highest – V_b values, Si6 and Si7, the coatings cracked and the formation of the large particles followed the cracks. This is displayed more clearly in Fig. 3 for Si6 (V_b = -100 V). The secondary electron image here together with the Si map show that the cracks propagated down to the Si substrate, which was then left exposed at those locations. Loss of the film may have also occurred from re-sputtering due to the energetic bombardment. It is not clear at this point what is the relation between the exposed Si substrate and the formation of macroparticles. However, it is evident that both, loss of the film in small locations and formation of macroparticles, are effects of the high – V_b applied and are clearly undesirable.

Regarding the bottom Al layer (b-Al), despite it was difficult to observe, in some instances when the top layers detached, some features of this layer could be analyzed. This is the case for the images of

Table 1
Details of the DOMS deposition experiments.

Sample Name	V_b [V]	P_a [kW]	V_p [V]	I_p [A]	Frequency (long pulses) [Hz]	Duty cycle (long pulses) [%]	Duty cycle (Oscillation pulses) [%]
Si1	Ground	1	493	67	774	75%	4.76
Si2	Floating	1	511	68	756	73%	4.76
Si3	-30	1	501	65	804	78%	4.76
Si4	-60	1	514	64	817	79%	4.76
Si5	-80	1	510	63	783	76%	4.76
Si6	-100	1	480	65	616	79%	4.76
Si7	-120	1	492	63	624	78%	4.76

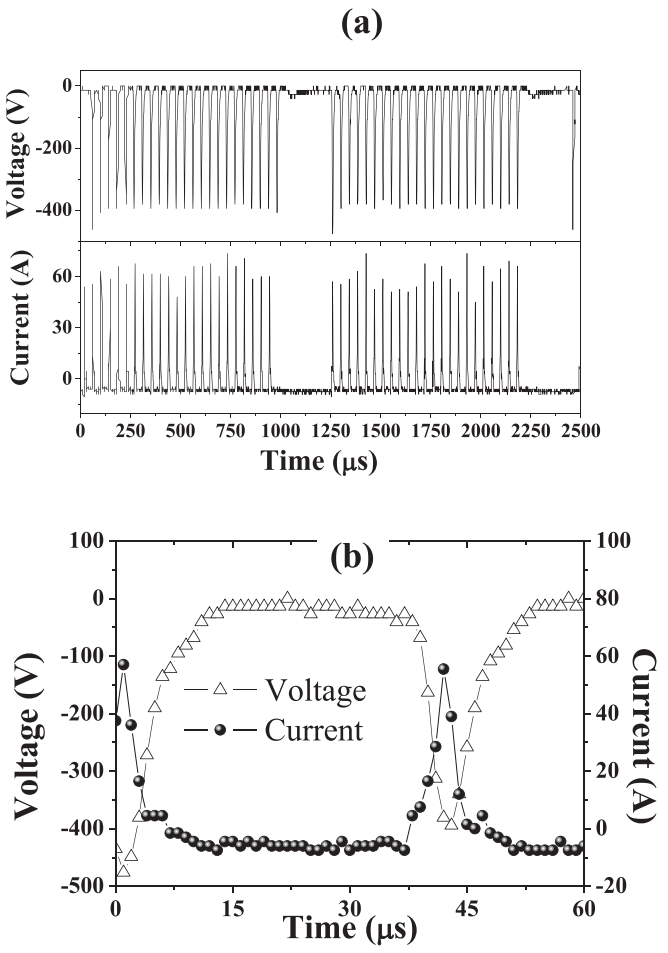

Fig. 1. (a) Waveforms of the target voltage and current variation for the long pulses and deep oscillation packets. (b) Detail of the target voltage and current within one oscillation.

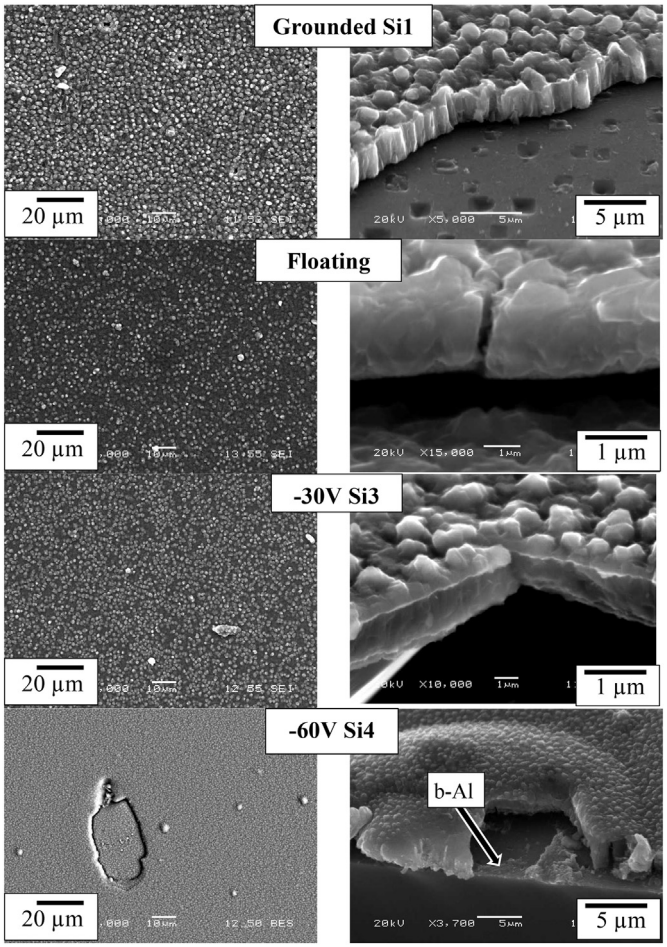

Fig. 2. SEM secondary electron images from the surface (left column) and cross-section (right column) of the b-Al/AlN/t-Al films for the seven bias voltage values used.

samples Si4, Si6, and Si7 on the right column of Fig. 2, where the b-Al was exposed and labeled with a black arrow. The images show that the morphology of this layer was different of that of the top Al film. The b-Al was finer and thinner than the t-Al and did not show the granular morphology observed in this film. Since both layers were deposited in the same conditions, the difference can be attributed to the influence of the substrate material (Si for b-Al and AlN for t-Al) on the nucleation and growth of the Al.

The results from AFM in Fig. 4 provided a quantitative assessment of the roughness as well as further details of the surface morphology. Two scans were obtained for each sample: a 5 μm by 5 μm scan and a 20 μm by 20 μm scan presented in the left and right columns of Fig. 4, respectively. In the 5 μm by 5 μm scans, it can be observed that the granules and the flatter regions on which they formed should correspond to Al nuclei growing on the surface of flatter AlN. The fact that the granules were separated, this is, they were not growing as a continuous front, may either indicate that the deposition time for the top Al layer was not long enough to reach coalescence of the nuclei, or that 3-D island nucleation and growth of Al on the AlN dominated [17]. In some instances, the Al granules showed facets, see for example the white arrows for sample Si3 in Fig. 4, which indicates that the adatom mobility was rapid enough to reach outer equilibrium shapes. As the -V_b increased, particularly from -60 V, the nuclei became smaller and closer together, i.e. higher nucleation rate was achieved. In samples Si6 and Si7 the large difference in Ra values for the small and large scanned regions reflects the contribution to roughness of the large particle agglomerations formed on the surface of these samples, which are only detected in the large scans.

Regarding the morphology of the AlN films, as observed in the AFM images, the surface of the AlN was much smoother than that of the t-Al

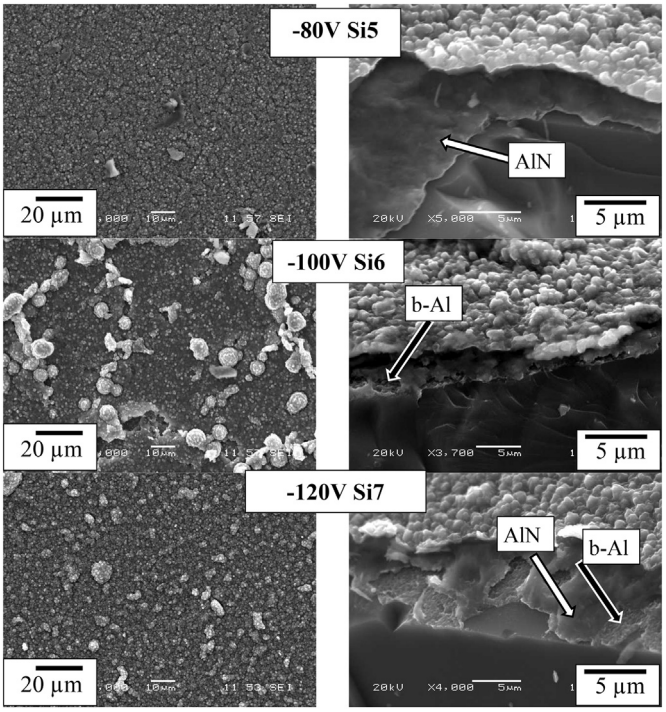

Fig. 2. (*continued*)

layer. This can also be seen in the secondary electron images of Fig. 2 in the regions where the top Al detached, see white arrows in the micrographs of samples Si5 and Si7. The flat surface morphology is indicative of fine columnar growth. This was indeed observed in the cross-sectional views of the low - V_b values samples, Si1 to Si3, in which fine columns grew tightly together to form a dense structure. For larger - V_b values, the columns were much less defined, and the film became more compact, this is the thickness of the films in general decreased with - V_b. It ranged from ~2.6 µm for the grounded sample down to ~1.1 µm for the sample produced at -120 V.

To investigate the composition of the films, XPS analysis was carried out in sample Si3. The results are presented in Fig. 5 as concentration profiles for Al, N, O, Si and C. Fig. 5(a) corresponds to the total sputtered depth and 5(b) is a detailed view near the surface. In 5(a), the depth sputtered from 0 to ~200 min, can be associated to the t-Al layer and showed a significant amount of N, which was also evident in Fig. 5(b). This N may have arisen from residual nitrogen in the chamber after the deposition of the AlN film. Beyond ~200 min of sputtering, the results correspond predominantly to the AlN film. One of the main observations here is that the Al and N contents were both close to 50 at. %, this is, the AlN was nearly stoichiometric. Another important feature in the XPS results was that the level of oxygen in the films was very low, which points to the relevance of a high vacuum level and ion cleaning of the substrate surface prior to deposition to produce oxygen-free AlN films.

In terms of film crystallinity and orientation, the GAXRD results presented in Fig. 6 show a strong effect of the bias voltage. As in the case of surface film morphology, two regimes in terms of the bias voltage were observed. For the film deposited at ground potential, several h-AlN reflections appeared where the (002) peak was quite low indicating little texturing of the film in this orientation. For floating potential and V_b = -30 V, preferential orientation along (002) increased strongly and the maximum (002) height corresponded to floating potential. For V_b = -60 V, the h-AlN (002) peak sharply decreased and it disappeared from -80 V onward. In these samples, the h-AlN (100) reflection was the most prominent. The width of this peak increased with – V_b, would suggest a continuous refinement of the film "grains" and/or the presence of non-uniform stress [18]. However, the large globular

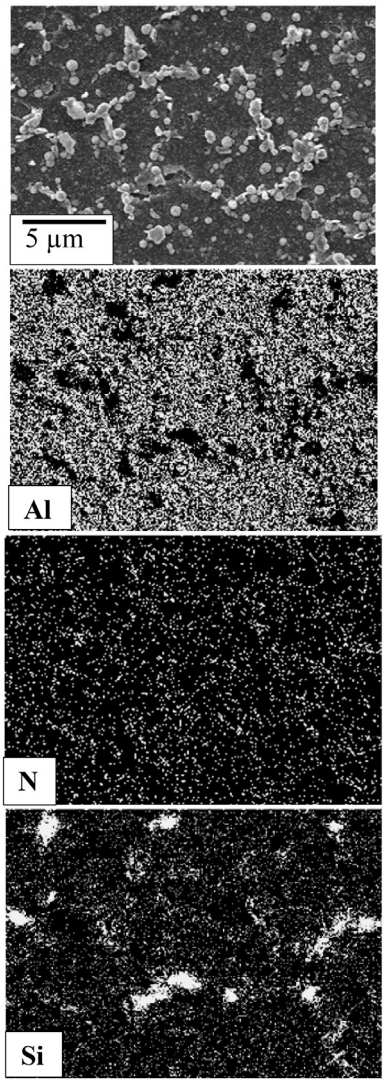

Fig. 3. SEM secondary electron surface view and corresponding Al, N, and Si x-ray maps from sample Si6 deposited at V_b = -100 V.

"grains" observed for these samples in Fig. 2, point more to the development of stress in these films. Furthermore, in contrast with the films obtained at lower - V_b, there were fewer h-AlN peaks in these samples indicative of loss of crystallinity. In all the samples, the main peaks of the AlN were slightly to the left of their standard positions, suggesting the presence of biaxial compressive stress. These results indicate that there was a small critical bias voltage range (floating to -30 V) outside which no benefits in terms of film orientation were obtained. Furthermore, around this value the level of residual stress was rather small.

Another important observation in the GAXRD results was that despite the cubic crystal structure of the b-Al layer on which the AlN was deposited, no cubic AlN (c-AlN) was found in any of the samples. This is in contrast with our previous studies of deposition of AlN via r.f. MS on Al adhesion layers [19] where a mixture of c-AlN and h-AlN was obtained. Thus, in the present experiments, the high adatom energy and mobility was able to overcome the "seed" effect of the cubic b-Al to attain the desired h-AlN phase.

In the case of the Al reflections, which should correspond to the top Al layer, all the Al peaks appeared with their relative intensities as in bulk polycrystalline Al regardless of the bias voltage used. This is the bias voltage did not lead to a preferential orientation in the t-Al film. In contrast, during deposition by DOMS of higher melting point metals

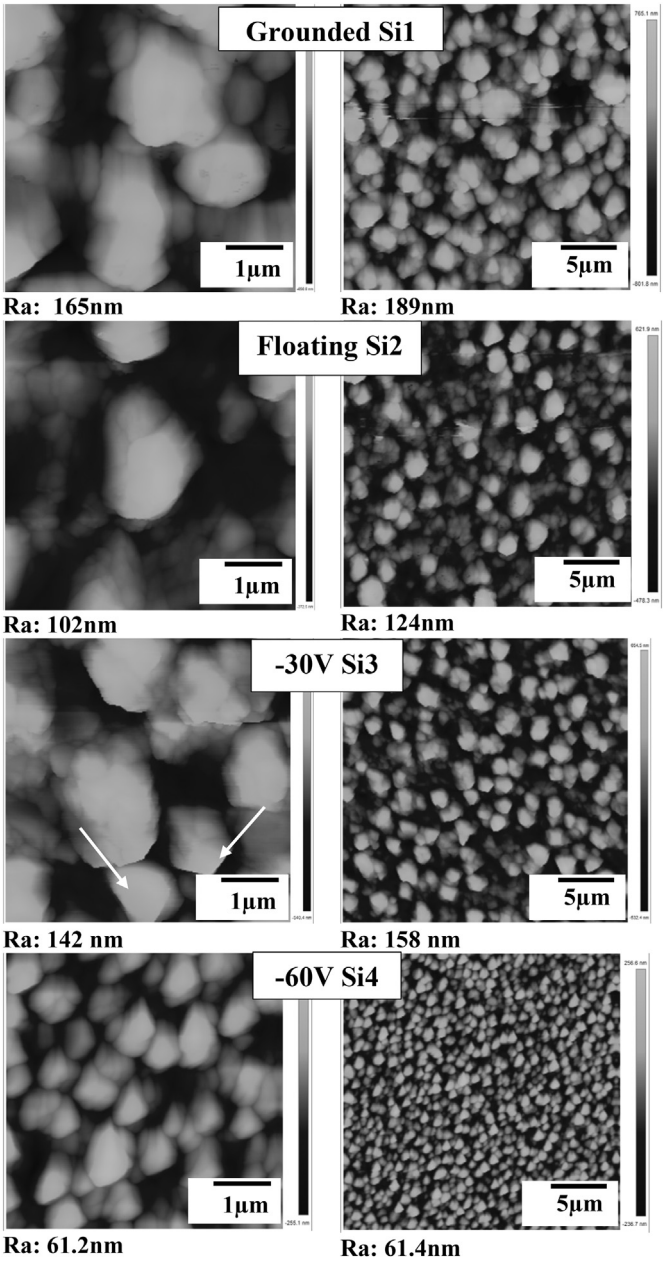

Fig. 4. AFM views from the surface of the b-Al/AlN/t-Al films for the seven bias voltage values used. Left column: 5 μm × 5 μm scan, right column: 20 m × 20 μm scan.

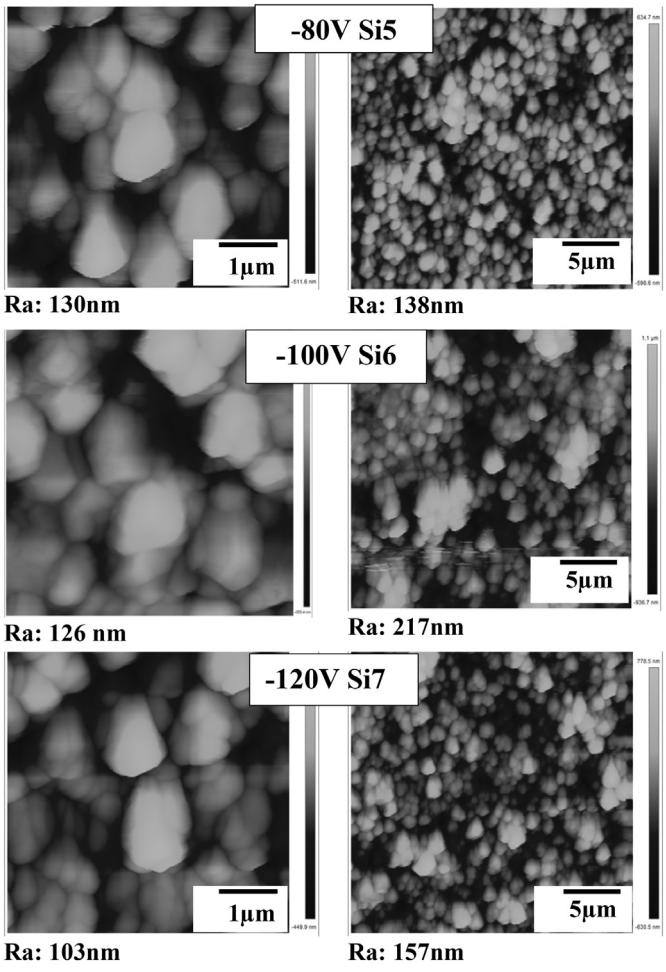

Fig. 4. (*continued*)

such as Cr [20] and Ta [14] a strong texture did develop. The difference may be related to different homologous temperatures in each case. The position of the Al peaks in all the samples showed a small and constant shift to the right of their bulk unstressed positions, suggesting the presence of similar compressive residual stress in the t-Al films for all V_b values. These stresses may arise from the N in solid solution observed in the XPS results and/or introduction of some defects in the Al crystal lattice with ion bombardment. Thermal stress due to the difference in thermal expansion coefficient with the AlN underneath may have also played a role.

Most of the observations presented in the previous section can be discussed in terms of the ion/particle bombardment of the growing film occurring in DOMS. The discussion can be divided in two regimes: low V_b (ground to -30 V) and high V_b (-60 V to -120 V). Since all the films were deposited at the same peak power level, it is assumed that the ionization fraction was similar in all cases and abundant enough to produce stoichiometric AlN films. However, the nature and energy of the arriving species should have been affected by the level of substrate voltage.

4. Low V_b regime

At low V_b, during the DOMS pulse-on period, hot secondary electron bombardment dominates. Furthermore, during the pulse-off period, the peak positive target current is expected to be low due to the weak attraction and acceleration of the positive ions by the small - V_b. As a result, the overall substrate current during a long pulse should be on the negative side [21]. The weak positive ion bombardment minimizes the generation of defects and residual stress, and results in the best features for the b-Al/AlN/t-Al films. The most important of these characteristics was the high crystallinity and the h-AlN (002) orientation obtained. This is a central requirement for sensors that rely on the piezoelectric effect, and none of the samples in the high V_b regime showed this feature. Thus, only a moderate energy of the arriving species was sufficient to attain good crystallinity and the equilibrium (002) texture of the h-AlN. This result also emphasizes the careful control of the type and energy of the arriving species to produce preferential orientation. As an additional advantage in this regime, the low energy ion bombardment resulted in a low level of compressive residual stress in these films, but good density at the same time. Formation of a ZT structure of tight, fine columnar grains was observed in these conditions. This result is consistent with the structure predicted by the diagram proposed by Anders [22], which includes the effects of particle bombardment.

Turning to the features of the top Al, the morphology observed suggests that the formation of this layer was dominated by the

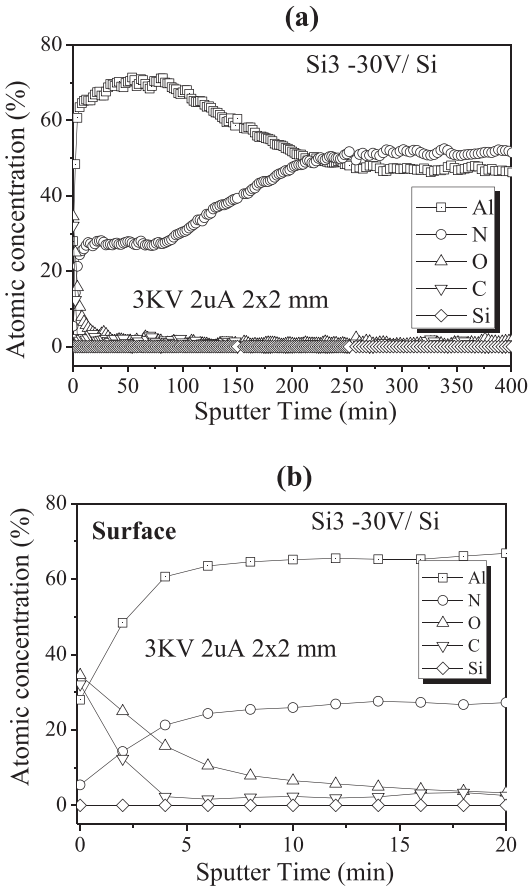

Fig. 5. (a) XPS profile of sample Si3 (V_b = -30 V), showing the contents of Al, N, O, C and Si from the surface into the sample for a sputtering time of 400 min. (b) Detail of the profile in (a) near the surface.

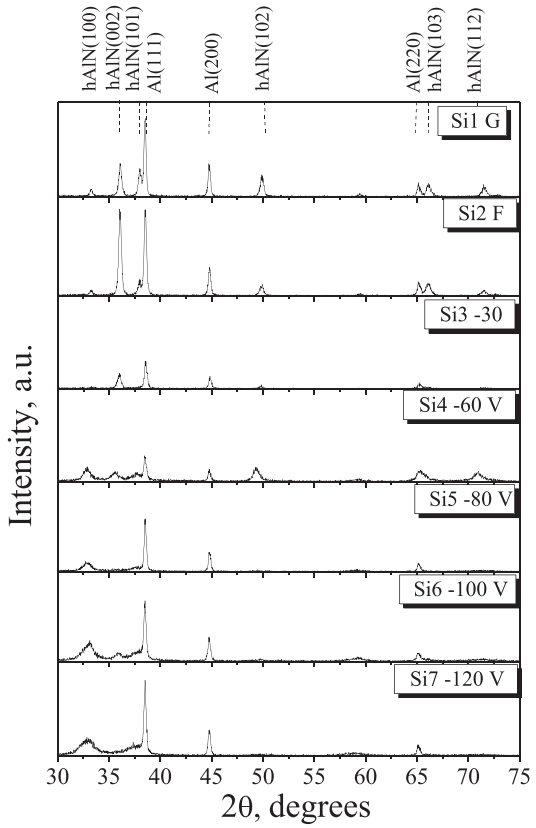

Fig. 6. GAXRD patterns from the surface of the b-Al/AlN/t-Al films for the seven bias voltage values used.

nucleation process. The surface morphology was composed of small nodules on a flat surface, which reflects a 3-D island nucleation and growth consistent with Al having much more affinity to itself than to AlN. Additionally, it seems that the hot secondary electrons may have provided some thermal energy that led to high homologous temperature (considering that in this case we are dealing with pure Al). As a result, growth occurred close to the recrystallized grain structure in the diagram of Anders [22], thus the non-columnar large globular grains observed in the Al films. Some refinement of this top morphology was observed as - V_b increased, likely as the breaking up of growing nuclei, but it was rather limited, confirming the lower energy of the ion bombardment in this regime. Finally, it is interesting to note that despite the increased energy of the adatoms in DOMS even at low V_b, the top Al, although clearly crystalline, did not develop any type of texture, only faceting in some of the Al grains was observed.

It remains to be seen whether the fine topography of the top Al layer observed in this regime, which is associated to the attaining of the best AlN features, will result in a good response during biofunctionalization. This is currently under investigation and will be reported in a forthcoming paper.

5. High V_b regime

In the high negative V_b regime, bombardment by hot secondary electrons drastically reduced, while a strong positive ion bombardment was favored. The high-energy bombardment by the large positive ions produced several surface and subsurface effects during nucleation and growth of the various layers.

In terms of the AlN structure, one of the most evident results of the abundant and energetic ion bombardment was the densification and compaction of the films. These features mainly arise from filling of voids by the enhanced forward adatom mobility given the significant momentum transfer from the energetic ions. Also, the high impact energy resulted in breaking-up of forming nuclei leading to higher nucleation rates and much finer columns. Even suppression of columnar growth may occur in these conditions [23], which indeed was observed in these films. However, the high impact energy also resulted in low crystallinity and absence of any type of texture in these samples. The high energy of the ions in this regime can cause several surface and subsurface effects including generation of crystalline defects such as vacancies, ion implantation, interstitial atoms, which lead to loss of crystallinity and in the extreme to the formation of amorphous structures.

The effect of the higher - V_b values on the Al top layer included a marked refinement of the surface morphology up to $V_b \sim$ -80 V. This refinement can be attributed to enhanced nucleation rate due to breaking of the forming nuclei. Beyond -80 V, an increase in surface roughness was observed due to the formation of the large Al particles agglomerates on the regions where the Si substrate was exposed. It is again interesting to note that the Al film crystallinity was not affected by the even higher energy ion bombardment in this regime. Thus, it seems that even if defects are created in the Al lattice, these are rapidly eliminated due to the high adatom mobility and the crystalline arrangement prevailed.

6. Conclusions

It is clear that the superior and versatile deposition capabilities of DOMS can produce Al/AlN/Al films on Si with excellent features for the development of acoustic biosensors. However, careful control of the deposition conditions is required. In particular, regarding the bias

voltage applied to the substrate, there is a critical small range which provides enough acceleration of ions towards the film surface to produce dense columnar AlN films and high secondary electron bombardment to provide the adatom mobility required to grow the (002) orientation. Outside this range, at lower - V_b values, not enough adatom mobility limits the formation of textures, and higher - V_b levels lead to excessive positive ion bombardment and loss of crystallinity in addition to higher residual stress.

The features of the top Al film were also affected by the bias voltage, mostly its morphology rather than its crystallinity or orientation. This points out to the difficulty of achieving simultaneously the best characteristics in each layer of a multilayer, multifunctional film, even with a powerful deposition technique such as DOMS.

Finally, it is important to mention that additional work is required to evaluate the response to biofunctionalization of the present films, which is central for biosensors. This will be part of a forthcoming study.

Acknowledgments

The authors would like to thank Roberto Carlos Vega-Morón from the Surface Engineering Group at SEPI ESIME, CDMX, México and Dr. Juan Vicente Méndez-Méndez from the Centro de Nanociencias y Micro y Nanotecnologías, CDMX, México, for their assistance in performing the XPS experiments. The help of Lázaro Huerta from the Instituto de Materiales de la UNAM, CDMX, México in performing the XPS experiments is also acknowledged.

References

[1] D.S. Ballantine Jr., S.J. Martin, A.J. Ricco, G.C. Frye, H. Wohltjen, R.M. White, E.T. Zellers, Chapter 3, 4 & 6 - Acoustic Wave Sensors and Responses, Appl. Mod. Acoust. Academic Press, Burlington, 1997, pp. 36–149, , https://doi.org/10.1016/B978-012077460-9/50003-4.

[2] M.I. Rocha-Gaso, C. March-Iborra, Á. Montoya-Baides, A. Arnau-Vives, Surface generated acoustic wave biosensors for the detection of pathogens: A review, Sensors 9 (2009) 5740–5769, https://doi.org/10.3390/s9095740.

[3] R.S. Naik, J.J. Lutsky, R. Reif, C.G. Sodini, A. Becker, H. Huggins Fetter, R. Miller, J. Pastalan, G. Rittenhouse, Y.H. Wong, Measurements of the bulk, c-axis electromechanical coupling constant as a function of a1n film quality, IEEE Trans. Ultrason. Ferroelectr. Freq. Control 47 (2000) 292–296, https://doi.org/10.1109/58.818773.

[4] K. Länge, B.E. Rapp, M. Rapp, Surface acoustic wave biosensors: A review, Anal. Bioanal. Chem. 391 (2008) 1509–1519, https://doi.org/10.1007/s00216-008-1911-5.

[5] N. Moll, E. Pascal, D.H. Dinh, J.P. Pillot, B. Bennetau, D. Rebière, D. Moynet, Y. Mas, D. Mossalayi, J. Pistré, C. Déjous, A Love wave immunosensor for whole E. coli bacteria detection using an innovative two-step immobilisation approach, Biosens. Bioelectron. 22 (2007) 2145–2150, https://doi.org/10.1016/j.bios.2006.09.032.

[6] Y.Q. Fu, J.K. Luo, N.T. Nguyen, A.J. Walton, A.J. Flewitt, X.T. Zu, Y. Li, G. McHale, A. Matthews, E. Iborra, H. Du, W.I. Milne, Advances in piezoelectric thin films for acoustic biosensors, acoustofluidics and lab-on-chip applications, Prog. Mater. Sci. 89 (2017) 31–91, https://doi.org/10.1016/j.pmatsci.2017.04.006.

[7] M.A. Moreira, I. Doi, J.F. Souza, J.A. Diniz, Electrical characterization and morphological properties of AlN films prepared by dc reactive magnetron sputtering, Microelectron. Eng. 88 (2011) 802–806, https://doi.org/10.1016/j.mee.2010.06.045.

[8] A. Ababneh, U. Schmid, J. Hernando, J.L. Sánchez-Rojas, H. Seidel, The influence of sputter deposition parameters on piezoelectric and mechanical properties of AlN thin films, Mater. Sci. Eng. B Solid-State Mater. Adv. Technol. 172 (2010) 253–258, https://doi.org/10.1016/j.mseb.2010.05.026.

[9] A.V. Singh, S. Chandra, G. Bose, Deposition and characterization of c-axis oriented aluminum nitride films by radio frequency magnetron sputtering without external substrate heating, Thin Solid Films 519 (2011) 5846–5853, https://doi.org/10.1016/j.tsf.2011.02.074.

[10] K. Li, H. Jin, D.M. Wang, Y.F. Tang, Preparation of AlN thin films for film bulk acoustic resonator application by radio frequency sputtering, J. Zhejiang Univ. Sci. A. 10 (2009) 464–470, https://doi.org/10.1631/jzus.A0820572.

[11] D. Lundin, K. Sarakinos, An introduction to thin film processing using high-power impulse magnetron sputtering, J. Mater. Res. 27 (2012) 780–792, https://doi.org/10.1557/jmr.2012.8.

[12] J. Lin, W.D. Sproul, R. Wei, R. Chistyakov, Diamond like carbon films deposited by HiPIMS using oscillatory voltage pulses, Surf. Coat. Technol. 258 (2014) 1212–1222, https://doi.org/10.1016/j.surfcoat.2014.06.061.

[13] J.C. Oliveira, F. Fernandes, F. Ferreira, A. Cavaleiro, Tailoring the nanostructure of Ti-Si-N thin films by HiPIMS in deep oscillation magnetron sputtering (DOMS) mode, Surf. Coat. Technol. 264 (2015) 140–149, https://doi.org/10.1016/j.surfcoat.2014.12.065.

[14] F. Ferreira, C. Sousa, A. Cavaleiro, A. Anders, J. Oliveira, Phase tailoring of tantalum thin films deposited in deep oscillation magnetron sputtering mode, Surf. Coat. Technol. 314 (2017) 97–104, https://doi.org/10.1016/j.surfcoat.2016.08.017.

[15] J. Lin, R. Chistyakov, C-axis orientated AlN films deposited using deep oscillation magnetron sputtering, Appl. Surf. Sci. 396 (2017) 129–137, https://doi.org/10.1016/j.apsusc.2016.11.025.

[16] O. Salas, J. Lin, L. Melo-Máximo, A.E. Murillo, D. Melo-Máximo, J. Oliva-Ramírez, Production of AlN thin films via deep oscillation magnetron sputtering for biosensors, Proc. 24th ABCM Int. Congr. Mech. Eng. (2017), https://doi.org/10.26678/ABCM.COBEM2017.COB17-0390 (Curitiba, PR, Brazil).

[17] D.L. Smith, Thin-film deposition: principles and practice, Chapter 5 - McGraw-Hill (New York), (1995).

[18] B.D. Cullity, Elements of x-ray diffraction, 2d ed. Chapter 9, Addison-Wesley Pub. Co, Reading, Mass, 1978.

[19] A. Murillo, L. Melo-Máximo, B. García-Farrera, O. Salas, D. Melo-Máximo, J. Oliva-Ramírez, K. García-Oviedo, L. Huerta, J. Oseguera, Development of AlN thin films for breast cancer acoustic biosensors, J. Mater. Res. Technol. (2018), https://doi.org/10.1016/j.jmrt.2018.02.007.

[20] F. Ferreira, R. Serra, J.C. Oliveira, A. Cavaleiro, Effect of peak target power on the properties of Cr thin films sputtered by HiPIMS in deep oscillation magnetron sputtering (DOMS) mode, Surf. Coat. Technol. 258 (2014) 249–256, https://doi.org/10.1016/j.surfcoat.2014.09.020.

[21] J. Lin, W.D. Sproul, Structure and properties of Cr2O3 coatings deposited using DCMS, PDCMS, and DOMS, Surf. Coat. Technol. 276 (2015) 70–76, https://doi.org/10.1016/j.surfcoat.2015.06.044.

[22] A. Anders, A structure zone diagram including plasma-based deposition and ion etching, Thin Solid Films 518 (2010) 4087–4090. doi:https://doi.org/10.1016/j.tsf.2009.10.145.

[23] R.F. Bunshah, Handbook of hard coatings: deposition technologies, properties and applications, Chapter 4 - Noyes Publications (Norwich, N.Y;Park Ridge, N.J), (2001).